Supporting Information

Reversible Polarization-Enabled Hydrogen Evolution Reaction on Two-Dimensional Ferroelectric $Cu_n(CrSe_2)_{n+1}$ Monolayers

Wenyuan Zhang[†1], Jingguo Wang[†2], Qi Wang[1], Yanling Si[2*], and Guochun Yang[1*]

[1] *State Key Laboratory of Metastable Materials Science & Technology and Hebei Key Laboratory of Microstructural Material Physics, School of Science, Yanshan University, Qinhuangdao 066004, China, Email: yanggc468@nenu.edu.cn*

[2] *School of Environmental and Chemical Engineering, Yanshan University, Qinhuangdao 066004, China, Email: siyl@ysu.edu.cn*

[†]*These authors contributed equally.*

Index **Page**

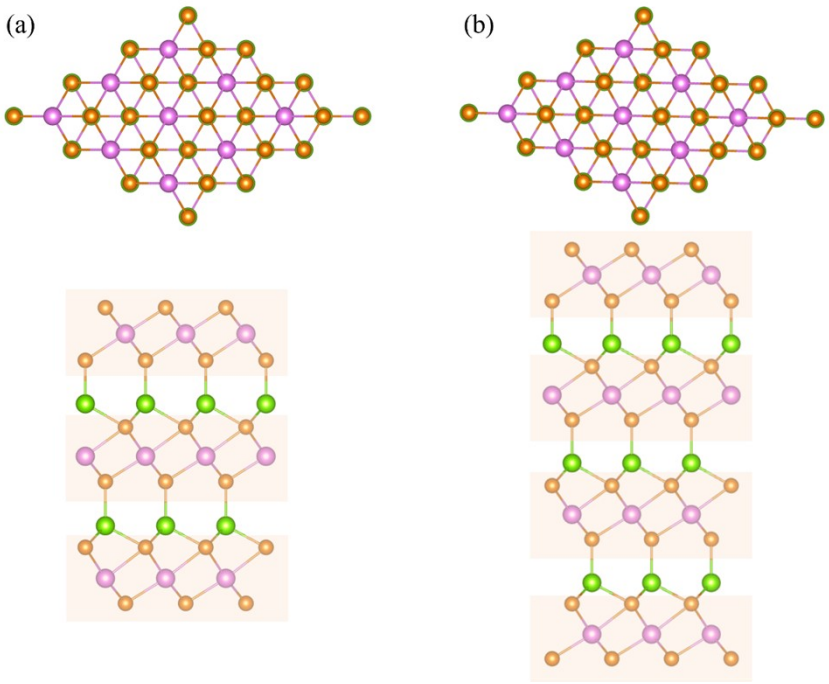

Fig. S1. (a-b) The top and side views of the structures of $Cu_2(CrSe_2)_3$ and $Cu_3(CrSe_2)_4$, respectively.

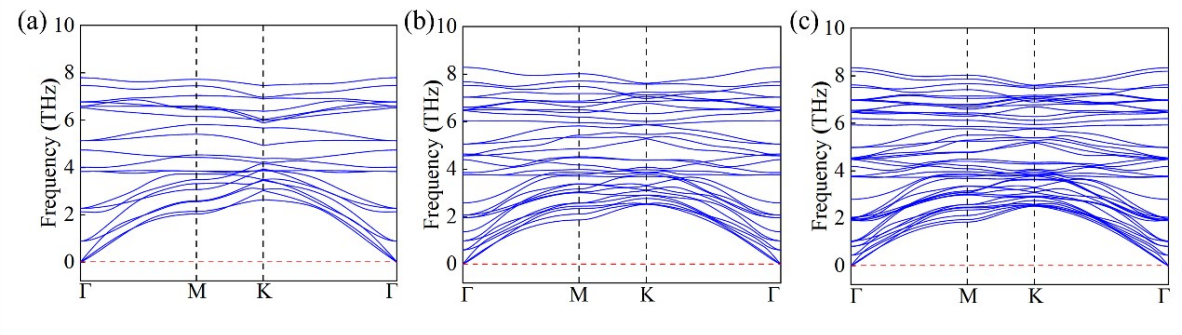

Fig. S2. The phonon spectra corresponding of $Cu_n(CrSe_2)_{n+1}$ (n = 1-3).

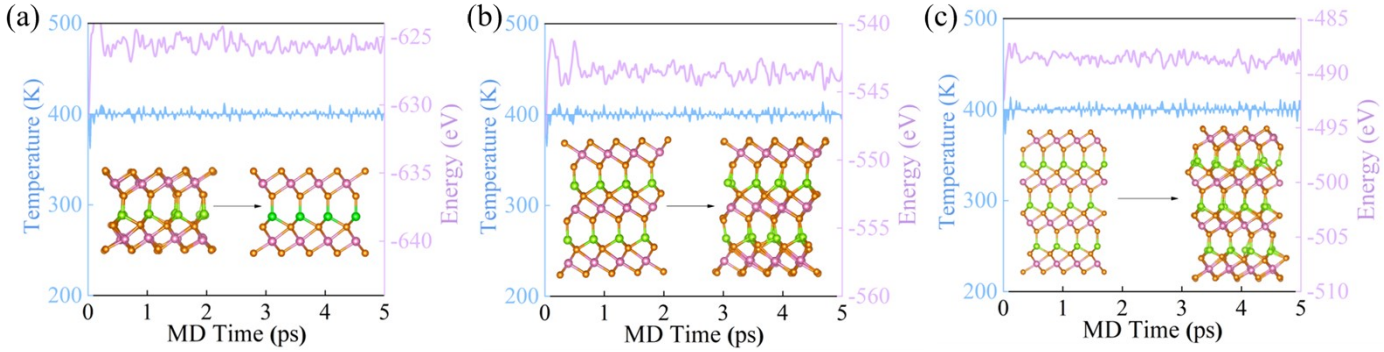

Fig. S3. Ab initio molecular dynamics simulations of $Cu_n(CrSe_2)_{n+1}$ (n = 1-3) at 400K for 5ps.

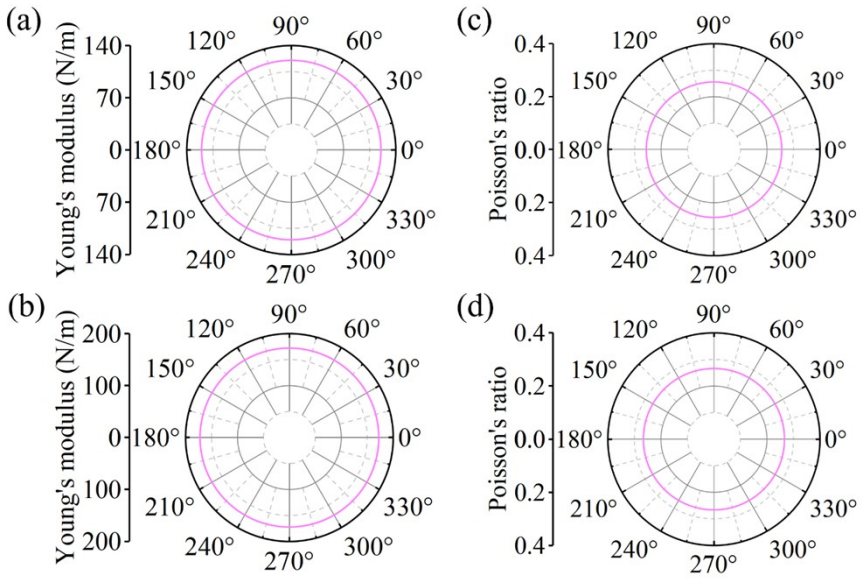

Fig. S4. The Young's modulus polar plots for $Cu_2(CrSe_2)_3$ and $Cu_3(CrSe_2)_4$ in panels (a-b) and the Poisson's ratio polar plots in panels (c-d).

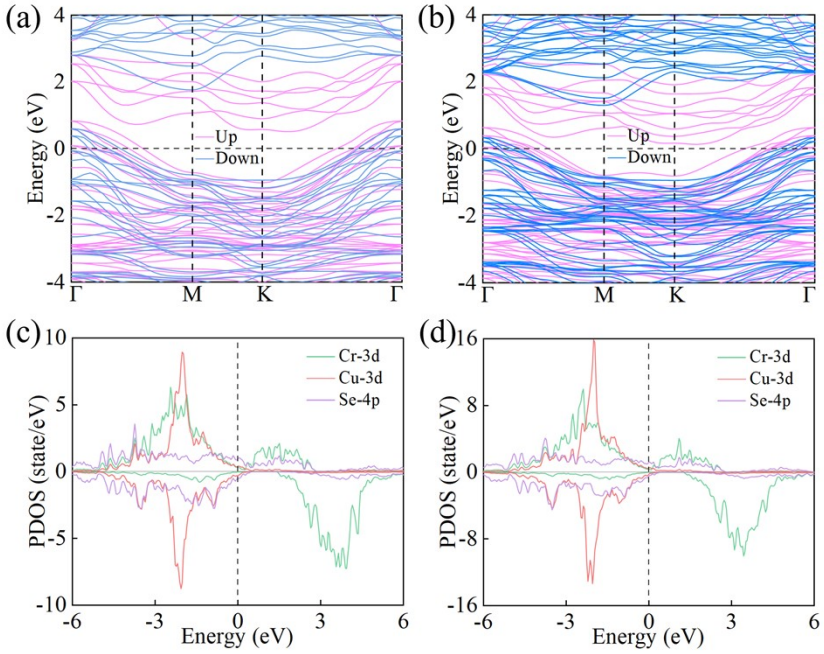

Fig. S5. (a-b) The electronic band structures of $Cu_2(CrSe_2)_3$ and $Cu_3(CrSe_2)_4$, respectively, while (c-d) present the corresponding projected density of states (PDOS).

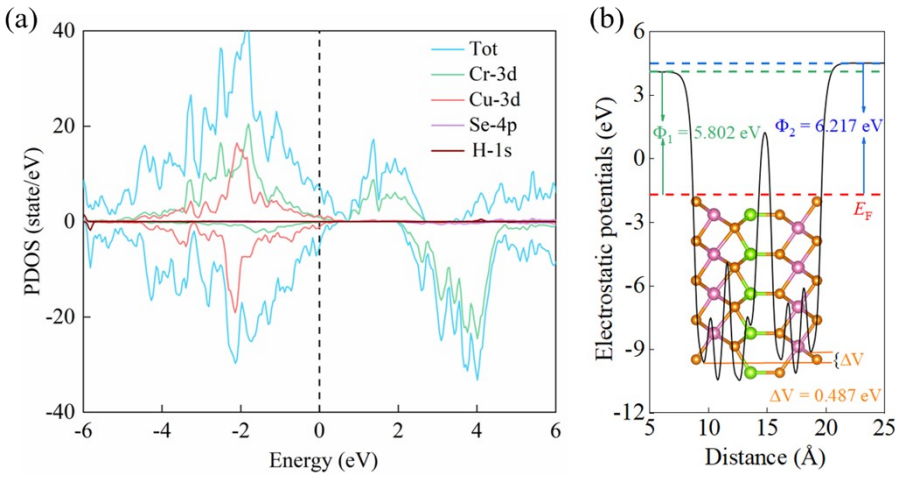

Fig. S6. (a) Projected density of states (PDOS) with H adsorption at the $T_{Se\,(D)}$ site in $Cu(CrSe_2)_2$. (b) Electrostatic potential, Fermi level (E_F), work function (Φ), and the potential difference (ΔV) of selenium (Se) atomic states between the upper and lower surfaces of $Cu(CrSe_2)_2$.

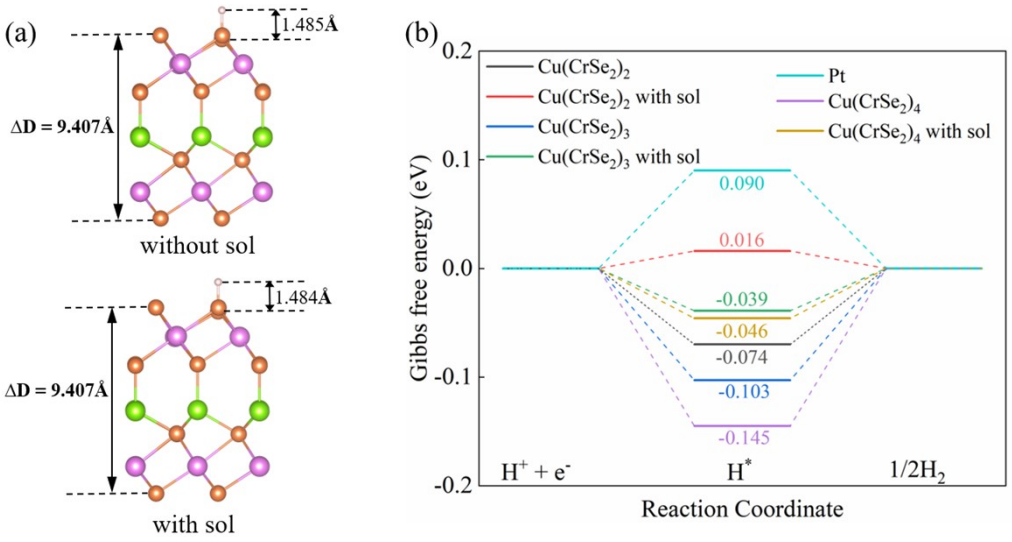

Fig. S7. (a) Optimized geometries of H adsorption at the T_{Se} (D) site of $Cu(CrSe_2)_2$ under solvent-free and solvent-included (with sol) conditions; (b) Corresponding ΔG_{H^*} at the T_{Se} (D) site of $Cu_n(CrSe_2)_{n+1}$ (n=1,2,3) under the respective conditions

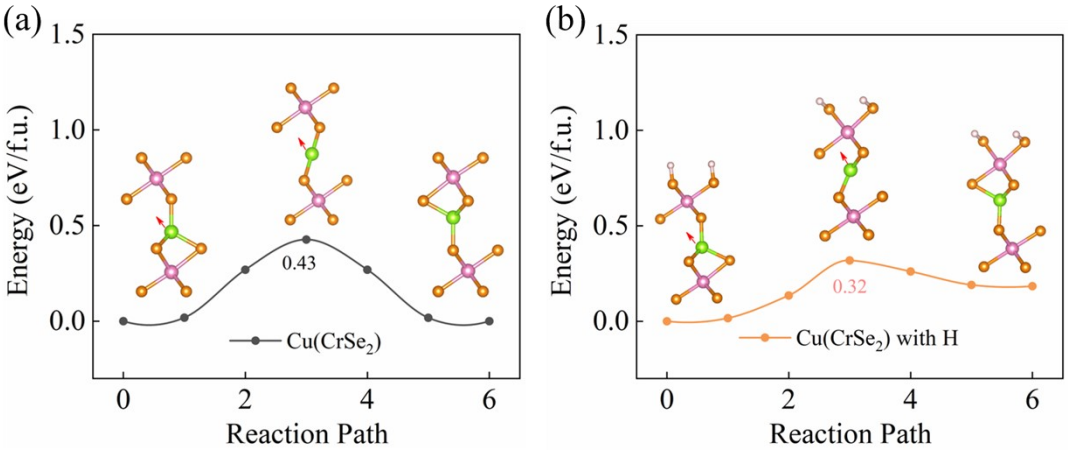

Fig. S8. Intrinsic ferroelectric polarization reversal pathway and associated energy barrier of $Cu(CrSe_2)_2$ mediated by Cu-ion migration in the pristine system (a), and the corresponding polarization reversal barrier after H adsorption (b). In the presence of adsorbed hydrogen, the energy profile becomes asymmetric: upon switching from the D-state to the U-state, the interaction between H and the surface is weakened, leading to an increase in the total energy of the U-state configuration with adsorbed H.

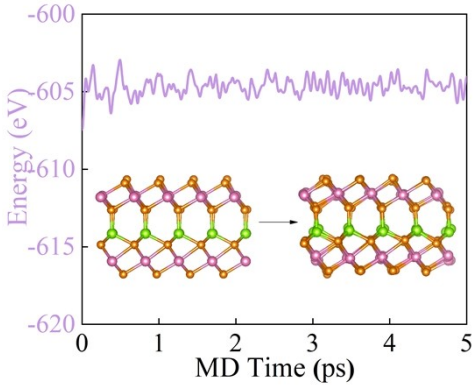

Fig. S9. Ab initio molecular dynamics simulations of $Cu_2(CrSe_2)_2$ after H desorption at 400K for 5ps.

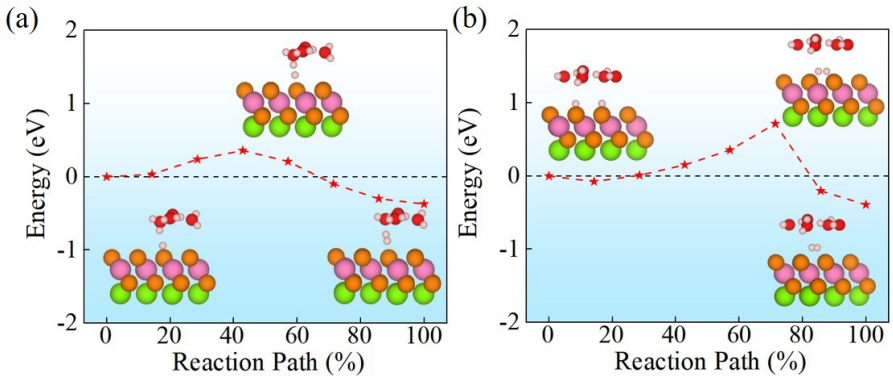

Fig. S10. The hydrogen evolution reaction mechanism on the top surface of $Cu(CrSe_2)_2$ in the upwards polarization (U) state: (a) Heyrovsky process, and (b) Tafel process, along with schematic diagrams of the corresponding reaction structures.

Table S1

Independent elastic constants (C_{ij}), Young's modulus (Y^{2D}) in N m^{-1} and Poisson's ratio (V^{2D}) of $Cu_n(CrSe_2)_{n+1}$ (n = 1-3).

	C_{11}	C_{12}	C_{66}	$Y^{2D}_{[01]}$	$Y^{2D}_{[10]}$	$V^{2D}_{[01]}$	$V^{2D}_{[10]}$
$Cu(CrSe_2)_2$	61.12	14.34	23.39	57.75	57.75	0.24	0.24
$Cu_2(CrSe_2)_3$	128.67	32.73	47.97	120.34	120.34	0.25	0.25
$Cu_3(CrSe_2)_4$	185.16	49.24	67.96	172.07	172.07	0.27	0.27

Table S2

The adsorption energy (ΔE_H) (eV) and Gibbs free energy (ΔG_{H^*}) (eV) of hydrogen on the adsorption sites of $Cu_n(CrSe_2)_{n+1}$ (n = 1-3) surfaces.

H site	**D**						**U**			
	T_{Se}		T_{Cr}		H_{SeCr}		T_{Se}		T_{Cr}	
	ΔE_H	ΔG_{H^*}	ΔE_H	ΔG_{H^*}	ΔE_H	ΔG_{H^*}	ΔE_H	ΔG_{H^*}	ΔE_H	ΔG_{H^*}
$Cu(CrSe_2)_2$	-0.31	-0.07	-0.14	0.10			0.12	0.36	0.27	0.51
$Cu_2(CrSe_2)_3$	-0.34	-0.10	-0.03	0.21	0.61	0.85	0.19	0.43	0.39	0.63
$Cu_3(CrSe_2)_4$	-0.38	-0.14	-0.13	0.11			0.16	0.40	0.36	0.60

Table S3. Average bond lengths of Se_2-Cr_1, Cu-Se_1, and Cu-Se_2 bonds in $Cu(CrSe_2)_2$ under zero electric field and ±0.5 eV/Å electric fields.

electric field strength (V/Å)	Bond length (Å)					
	$Cu(CrSe_2)_2$			$Cu(CrSe_2)_2$ with H		
	Se_2-Cr_1	Cu-Se_1	Cu-Se_2	Se_2-Cr_1	Cu-Se_1	Cu-Se_2
-0.5	2.531	2.306	2.420	2.541	2.326	2.425
0	2.530	2.307	2.418	2.539	2.327	2.423
0.5	2.526	2.312	2.416	2.536	2.329	2.421

Table S4. The differences in the lattice parameters and interlayer distance (d_{inter}) of $Cu(CrSe_2)_2$ calculated under zero electric field and ±0.5 eV/Å electric fields.

electric field strength (V/Å)	lattice parameters and d_{inter} (Å)					
	$Cu(CrSe_2)_2$			$Cu(CrSe_2)_2$ with H		
	a	b	d_{inter}	a	b	d_{inter}
-0.5	3.576	3.576	9.588	3.712	3.756	9.085
0	3.575	3.575	9.582	3.712	3.756	9.091
0.5	3.576	3.576	9.585	3.710	3.756	9.114

Table S5

Structural information of $Cu_n(CrSe_2)_{n+1}$ (n = 1-3).

Phase	Space Group	Lattice Parameters (Å, °)	Wyckoff Positions (fractional)			
			Atoms	*x*	*y*	*z*
$Cu(CrSe_2)_2$	*P*3*m*1	*a* = 3.58	Cu (1a)	0.00	0.00	0.46
		b = 3.58	Cr (1a)	0.00	0.00	0.36
		c = 30.00	Cr (1b)	0.33	0.67	0.58
		α = 90.00	Se (1a)	0.00	0.00	0.53
		β = 90.00	Se (1b)	0.33	0.67	0.41
		γ = 120.00	Se (1c)	0.67	0.33	0.31
			Se (1c)	0.67	0.33	0.63
$Cu_2(CrSe_2)_3$	*P*3*m*1	*a* = 3.63	Cu (1a)	0.00	0.00	0.60
		b = 3.63	Cu (1c)	0.67	0.33	0.38
		c = 30.00	Cr (1a)	0.00	0.00	0.50
		α = 90.00	Cr (1b)	0.33	0.67	0.72
		β = 90.00	Cr (1c)	0.67	0.33	0.29
		γ = 120.00	Se (1a)	0.00	0.00	0.67
			Se (1a)	0.00	0.00	0.34
			Se (1b)	0.33	0.67	0.56
			Se (1b)	0.67	0.33	0.24
			Se (1c)	0.67	0.33	0.77
			Se (1c)	0.67	0.33	0.46

		a =3.65	Cu (1a)	0.00	0.00	0.65
		b = 3.65	Cu (1b)	0.33	0.67	0.31
		c = 38.52	Cu (1c)	0.67	0.33	0.48
		α = 90.00	Cr (1a)	0.00	0.00	0.57
		β = 90.00	Cr (1b)	0.33	0.67	0.74
		γ = 120.00	Cr (1b)	0.33	0.67	0.24
$Cu_3(CrSe_2)_4$	*P*3*m*1		Cr (1c)	0.67	0.33	0.41
			Se (1a)	0.00	0.00	0.71
			Se (1a)	0.00	0.00	0.45
			Se (1a)	0.00	0.00	0.20
			Se (1b)	0.33	0.67	0.62
			Se (1b)	0.67	0.33	0.37
			Se (1c)	0.67	0.33	0.78
			Se (1c)	0.67	0.33	0.54
			Se (1c)	0.67	0.33	0.28